


Development and Optimization of Oral Dissolution Films for Enhanced Delivery of Ebastine-Loaded Solid Lipid Nanoparticles

Kai Chen^{1,2}, Yong Sun¹ 

¹Department of Pharmaceutics, School of Pharmacy, Qingdao University, Qingdao, 266021, People's Republic of China; ²Pharmacy Department, Affiliated Hospital of Jining Medical University, Jining, 272000, People's Republic of China

Correspondence: Yong Sun, Email chenkai4230@163.com; sunyong@qdu.edu.cn

Introduction: Approximately 10–30% of the worldwide population suffers from allergic diseases. Although ebastine (EBT) is described as a potential treatment for allergies, its effects are compromised due to poor solubility and low bioavailability.

Methods: This study introduced a novel delivery platform for ebastine by combining solid lipid nanoparticles (SLNs) with oral dissolution films (ODFs). Ebastine SLNs were fabricated using hot melt and ultrasonic emulsification methods, and the SLNs' formulation was optimized by a central composite rotatable design. The developed SLNs were further introduced into a mixed polymer solution of PVA and HPMC to prepare ODFs using the solvent casting method.

Results: The optimized EBT-SLNs with spherical structures demonstrated nanoparticle size (147.5 ± 3.32 nm), low polydispersity index (PDI, 0.106 ± 0.005), high entrapment efficiency (86.7%), as well as drug loading (10.02%), respectively. The optimum formulation of ODFs was composed of equal proportion of HPMC and PVA according to normalization methods by evaluation of physicochemical properties including physical appearance, folding endurance and disintegration time. Scanning electron microscopy results disclosed that EBT-SLNs were confined within the network of ODFs and no aggregation SLNs was found. Reconstitution experiments showed EBT-SLNs were still within the nanometers range and maintained a homogenous state, suggesting that incorporation of SLNs into ODFs not compromised their nanoparticulate properties. The in vitro drug release patterns from ODFs containing EBT-SLNs exhibited a fast release profile compared to the commercial EBT tablets.

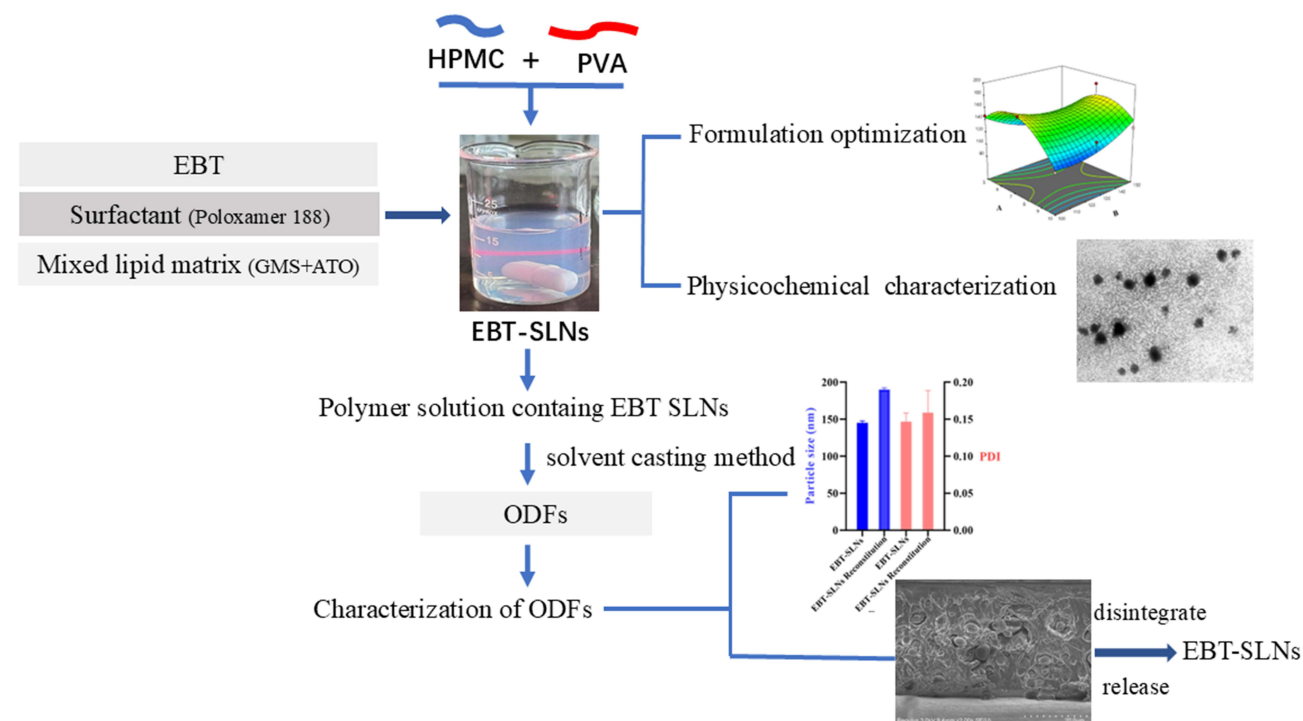
Discussion: The developed system demonstrates enhanced solubility, stability, and bioavailability of ebastine, offering a promising alternative to traditional oral tablets, with potential advantages in patient compliance and rapid drug onset. Therefore, the ODFs containing SLNs can be considered as an efficient approach for EBT administration.

Keywords: ebastine, solid lipid nanoparticles, oral dissolution films, central composite rotatable design

Introduction

Approximately 10% to 30% of the worldwide population suffers from allergic diseases. In these currently available drugs, ebastine (EBT), as a potent second-generation H1 histamine receptor antagonist, is commonly recommended for treatment of a wide range of allergies, such as rhinitis, urticaria and allergic contact dermatitis.^{1,2} Although oral delivery of ebastine is preferred, its therapeutic effect is compromised due to its poor water solubility, which limits absorption in physiological fluids and results in inadequate therapeutic function. As far as a BCS-II drug is concerned, it is reported that there is only about 40% bioavailability of ebastine is achieved after oral administration.³ Furthermore, the traditional oral administration method fails to convincingly improve its bioavailability, as the complex gastrointestinal environment and the first pass effect often cause irregular drug absorption and fast elimination, respectively. Therefore, exploring a novel drug delivery system for ebastine is essential to overcome these constraints associated with conventional oral dosage forms.

Graphical Abstract



At present, some formulations including fast disintegrating tablets,⁴ nanoparticle-based drug carriers, such as solid lipid nanoparticles (SLNs),⁵ micelles,⁶ microemulsions⁷ and transfersomes,³ have been used to deliver ebastine to increase solubility and further enhance its biopharmaceutical performance.

Among these approaches, fabrication of ebastine into SLNs is one of the more promising methods because this formulation has the advantages to enhance drug's stability, increase its absorption, and provide good biocompatibility. Furthermore, choosing SLNs as vehicles is appropriate for delivery of ebastine owing to the matrices of SLNs made up of solid lipids, which are especially preferred for loading lipophilic active pharmaceutical ingredients.^{8,9} Recent studies have demonstrated enhanced pharmacokinetic profiles when encapsulating ebastine into SLNs, which underscored the potential of using this strategy to improve its performance.⁵

Nevertheless, the dispersion of SLNs in the aqueous phase also faces a series of unstable problems such as drug leakage, aggregation and sedimentation during the preparation and/or storage procedure of SLNs, which are commonly encountered in liquid preparations.¹⁰ Therefore, converting the liquid SLNs into solid preparation becomes an attractive approach to solve the aforementioned limitations.¹¹ The development of oral dissolution films (ODFs), which are thin films that dissolve quickly in the mouth, has garnered significant attention in recent years.^{12–14} These types of films offer an alternative to conventional solid dosage forms and represent a significant advancement in oral drug delivery systems.¹⁵ ODFs are ultra-thin, stamp-sized films that offer several advantages over traditional tablets or capsules, including improved patient compliance, easier administration and enhanced bioavailability.¹⁶ The basic substrates of ODFs are often composed of certain hydrophilic film-forming agents such as pullulans, sodium alginate, hydroxypropyl methylcellulose (HPMC) and polyvinyl alcohol (PVA), etc.^{17–22}

Once placed in the oral cavity, ODFs can rapidly disintegrate or dissolve upon contact with saliva instead of requiring mastication or drinking extra water.¹⁵ The rapid disintegration of ODFs leads to an immediate onset of action, enhancing the oral absorption of low bioavailability drugs. When active drugs are loaded in ODFs, they can quickly release and be

absorbed through the oral mucosal membrane or buccal epithelium, avoiding first-pass metabolism and reducing the impact of the gastrointestinal environment.²³

While both SLNs and ODFs are known for advancing delivery systems, the integration of SLNs into ODFs for ebastine delivery has not been widely explored. Given the advantages of SLNs and ODFs, a hypothesis was proposed to create a composite delivery system. SLNs in ODFs could potentially solve the challenges of SLNs in liquid forms, such as aggregation and instability, while also addressing the poor bioavailability of ebastine. This system would use ODFs as a platform to incorporate SLNs for the oral delivery of ebastine. We thought that this combination could produce a synergistic effect both better the solubility of ebastine after encapsulating them into SLNs and address the unstable problem of SLNs after incorporating them into ODFs. This combination can leverage the unique properties of each system, potentially providing a novel system to deliver ebastine in specific clinical scenarios such as pediatric or geriatric populations or those patients with swallowing difficulties.

Hence, in this study, ebastine-loaded SLNs were first fabricated according to hot melt and ultrasonic emulsification methods, and the formulation was screened by a two-factor three-level central composite rotatable design method. Then the ODFs loaded with optimized SLNs were tailored by the solvent casting method. Moreover, the developed ODFs loaded with SLNs were evaluated for their physicochemical properties. The objective of this study is to develop and optimize oral dissolution films incorporating ebastine-loaded solid lipid nanoparticles to enhance their bioavailability, stability, and therapeutic effect.

Materials and Methods

Materials

Ebastine and glyceryl monostearate (GMS) were purchased from the Shanghai Aladdin Scientific Co. Ltd. Compritol 888 ATO and Poloxamer 188 were received from Beijing Fengli Jingqiu Pharmaceutical Co. Ltd. Hydroxypropyl methylcellulose (HPMC) was gifted from Shang Hai Colorcon Incorporation. Polyvinyl alcohol (PVA) was obtained from Sigma Aldrich. All other used reagents and chemicals were of analytical or chromatographic grade.

Methods

Fabrication of Ebastine-Loaded Solid Lipid Nanoparticles (SLNs)

The ebastine-loaded SLNs were fabricated according to the hot emulsification and ultrasonication homogenization method.²⁴ Briefly, the lipid materials composed of Compritol 888 ATO and glyceryl monostearate (GMS) were heated at 80°C to form a clear molten lipid solution, then ebastine was subsequently added until it was completely dissolved, which termed as oil phase. The poloxamer 188 as surfactant was dissolved in distilled water and heated to the same temperature of the oil phase. After mixing them together, the developed primary oil-in-water coarse emulsion was sonicated for 10 minutes at 400 W (worked for 3 seconds and paused for 2 seconds) to form nanoemulsions using a probe sonicator (JY92-II, Ningbo Scientz Biotechnology Co., Ltd., China). Finally, the ebastine-loaded SLNs were obtained by rapidly immersing the hot nanoemulsions into an ice bath at 0°C.²⁵ The blank solid lipid nanoparticles were prepared similarly except for addition of ebastine in the formulation.

Experimental Design

It is challenging to find an optimal formulation through a single-variable experiment because optimization of SLNs involves many variables and complex interactions among the factors. Thus, determining the critical parameters and optimizing the formulation is an important topic for discussion. Central composite rotatable design (CCRD) has been widely used in pharmaceutical formulation design because it can provide more information using a relatively limited number of experiments.^{26,27}

A two-factor three-level central composite rotatable design (CCRD) was used in this study to screen the optimal formulation of ebastine-loaded SLNs. The effect of two independent factors including the ratio of drug amount to lipid amount (X_1) and the amount of surfactant (X_2) on four dependent responses such as particle size (Y_1), polydispersity

Table 1 Independent Factors and Their Levels Used in CCD

Independent Factors	Levels		
	Low	Medium	High
X_1 : the ratio of lipid to drug	5	7.5	10
X_2 : the amount of surfactant	100	125	150
Dependent response		Constraints	
Y_1 : particle size (nm)		Minimize	
Y_2 : polydispersity index		Minimize	
Y_3 : entrapment efficiency (%)		Maximum	
Y_4 : drug loading (%)		Maximum	

index (Y_2) entrapment efficiency (Y_3 , EE) and drug loading (Y_4 , DL) were investigated. The independent factors and their levels used in the study were shown in Table 1.

To accurately describe the obtained results, the responses from the thirteen experimental runs were fitted into several mathematical models, including the linear, two-factor interaction and quadratic models. This fitting was based on the analysis of variance for p -values, with values less than 0.05 considered statistically significant. To predict the optimal formulation, a target function was generated according to the predetermined constraints, setting the values for particle size and PDI to their minimal level, while aiming for maximum values for EE and DL. The ebastine-loaded SLNs based on the selected optimum formulation were prepared for further study in the follow-up experiments.

Characterization of Ebastine-Loaded SLNs

Particle Size, Zeta-Potential and Morphology

Particle size, zeta-potential and polydispersity index (PDI) of the prepared ebastine-loaded SLNs were determined using a Zetasizer Nano instrument (Nano ZS90, Malvern Instruments Ltd., UK). The morphology of ebastine-loaded SLNs was observed by transmission electron microscopy (TEM) (JEM 2010HE, JEOL, Japan).

Entrapment Efficiency and Drug Loading

To assess the EE and DL of ebastine-loaded SLNs, after introducing 1.0 mL of the prepared ebastine-loaded SLNs into an ultra-centrifugal filter tube (Millipore, cut off MW 3KD), the unencapsulated ebastine was determined in the outer tube after centrifugation at 5000 rpm for 20 mins. The absorbance of ebastine was measured at 259 nm. The content of ebastine was then calculated using a previously established linear regression equation. The entrapment efficiency and drug loading were determined by the following equations:

$$EE\% = \frac{\text{added total drug}(mg) - \text{unentrapped drug}(mg)}{\text{added total drug}(mg)} \times 100\%$$

$$DL\% = \frac{\text{added total drug}(mg) - \text{unentrapped drug}(mg)}{\text{added total lipid and entrapped drug}(mg)} \times 100\%$$

Fourier Transform Infrared Spectroscopy (FTIR)

The chemical structure of ebastine dispersed in the SLNs was analyzed by Fourier transforms infrared (FTIR). After the different samples, such as ebastine, drug-free SLNs, ebastine-loaded SLNs, the physical mixture of drug-free SLNs and ebastine, were grinded homogeneously with potassium bromide separately, the obtained mixtures were compressed into transparent pellets and put them in the FTIR spectrometer apparatus (IRAffinity-1S, Shimadzu, Japan) for analysis. The scanning range was arranged from 4,000 cm^{-1} to 400 cm^{-1} with the resolution was 4 cm^{-1} .

Preparation of ODFs Containing Ebastine-Loaded SLNs

To better deliver ebastine and devoid of the shortcoming of liquid preparations, after successful fabrication of ebastine-loaded SLNs with smaller particle size and higher EE% and DL%, ebastine-loaded SLNs embedded in ODFs were further developed. Since film-forming polymers are crucial for producing ODFs, two commonly used materials, such as hydroxypropyl methylcellulose (HPMC) and polyvinyl alcohol (PVA), were recommended as the matrix for the film. The ODFs were produced by the conventional solvent casting method.^{28,29}

Briefly, various ratio of PVA and HPMC were dissolved in distilled water to form clear solution formed. Then, other excipients, such as plasticizer (glycerol), sweetener (sucrose), and flavor agent (orange flavor) were separately added into the polymer solution under continuous stirring. After removing the air bubbles, the degassed homogeneous solution was cast onto a glass plate and left to dry in an air circulating oven at 40°C for 24 h. Finally, the properties of the ODFs, including film forming capability, surface roughness, peel ability, uniformity, folding endurance and disintegration time, were investigated as evaluating indicators to optimize the formulation of ODFs.³⁰

Folding Endurance Test

To evaluate the mechanical properties of the prepared films, the folding endurance experiment was explored by continuously folding the film along its central line until it cracked or broke.^{31,32} The folding endurances were recorded as any cracks or fractures presented at the folding site. The tests were performed in triplicate, and the results were reported as the mean \pm standard deviation (SD).

Disintegration Test

The disintegration experiment was conducted using Petri dish method.³³ A film measuring 2 cm² was placed into a glass dish filled with 5 mL of artificial saliva solution (pH 6.8), which was preheated to 37°C. Then, the dish was shaken at a speed of 10 rpm at 37°C to simulate the oral conditions. The disintegration time was defined when the film first contacts the medium until it is fully dissolved, without no visible residue.³⁴ The tests were performed in triplicate, and the values were presented as mean \pm standard deviation (SD).

Characterization of ODFs

pH Measurements

Before drying the films, the pH of the ODFs solution with different formulations was measured using a pH meter (P13, YOKE instrument company, Shanghai, China). The samples were performed in triplicate, and the results were expressed as mean \pm standard deviation (SD).

Film Thickness & Weight Measurement

After cutting into a square size with a 2 cm² surface area, the prepared films were checked for thickness homogeneity and weight variation. The thickness of the films was measured at five locations using a digital Vernier caliper: one at the intersection of the diagonals and four at the midpoints of the rectangle's edges. Weight variation of the films was evaluated using a digital analytical balance (BT25S, Sartorius, Germany). Each film was precisely weighed. The experiments were conducted in triplicate and mean \pm standard deviation (SD) was calculated.

Surface Morphology of Films

To learn how SLNs distributed into ODFs and probe whether SLNs aggregated or not during the ODFs preparation process, the surface micromorphology and microstructure of the prepared films was observed by field emission scanning electron microscopy (FESEM, Regulus8100, Hitachi, Japan), aiming to learn the distribution of SLNs in ODFs and their aggregation during preparation. The film sample was fixed by carbon conductive glue and gold coating before scanning.

Reconstitution of Ebastine-Loaded SLNs in ODFs

The particle size and polydispersity index (PDI) of the SLNs before and after their incorporation into the films were compared to determine if they could be effectively redispersed upon release from the ODFs. After the ODFs integrated

with ebastine-loaded SLNs were completed dissolved in artificial saliva fluid, the reconstruction of SLNs was evaluated for the particle size and PDI.

Content Uniformity Determination

A validated high-pressure liquid chromatography (HPLC) method was employed to measure content and assess content uniformity. The HPLC condition for the determination of EBT included a C18 reverse-phase column (200 mm × 4.6 mm, 5 µm; Hypersil ODS, YILITE Da Lian, China), and the detected UV wavelength was set at 259 nm. The mobile phase was composed of acetonitrile and 0.02 mol/L of phosphoric acid solution (75:25, v/v, adjusting pH to 6.0 using triethylamine) with a constant flow rate of 1.0 mL/min and the determination temperature was kept at 25°C. Briefly, a random film sample from three different batches was accurately weighted and dissolved with mobile phase, then diluted to 10.0 mL in a volumetric flask. After sonication for 15 min, the extracted solution including ebastine was filtered through a 0.22 µm filter to prepare the sample for HPLC analysis.

The content of ebastine in the film was calculated using already established calibration curve with known gradient ebastine concentrations. Content uniformity was then evaluated using the equation: $A + 2.2S$, where A represented the absolute value of the difference between 100 and the average concentration $|100 - \bar{x}|$, and S denoted the standard deviation.

In vitro Release Study

The In vitro drug release profile of ebastine from ODFs loaded with ebastine SLNs was studied using dissolution apparatus (RCZ-6C4, Shanghai Huanghai Medicament Test Instrument Factory, China) applying the basket method. The film was cut into per-unit doses and placed in the basket device. A 100 mL of artificial saliva solution (pH 6.8) was used as the dissolution medium, preheated to $37 \pm 0.5^\circ\text{C}$, with a stirring speed maintaining at 50 rpm. At intervals 5, 10, 15, 30, 45 and 60 min, a 5.0 mL sample was withdrawn and replaced with an equal volume of pH 6.8 artificial saliva solution, which was maintained at the same temperature. After filtration, the absorbance of each sample was determined at 259 nm wavelength with a UV spectrophotometer (X-8, Metash, Shanghai, China). The percentage cumulative release was calculated using a previously prepared calibration curve. All samples were performed in triplicate.

Results and Discussion

Fitting the Response Models

Preliminary studies disclosed that two independent factors, including the ratio of lipid to drug and the amount of used surfactant, had a vital influence on the selected dependent response. In this study, the values of particle size, PDI, EE and DL across the 13 runs ranged from 104.1 nm to 185.5 nm, 0.079 to 0.305, 78.78% to 92.18% and 6.56% to 11.94%, respectively. Based on these results, various mathematical models, such as linear, two-factor interaction (2F) and quadratic models, were, respectively, fitted according to various statistical analyses.

The model summary statistics for the selected responses, presented in Table 2, suggested that the quadratic model was the most appropriate for analyzing the independent variables, because this model had the least SD values, predicted residual sum of square (PRESS), as well as the maximum R^2 , indicating a good fit. Focusing on the model whose adjusted R^2 and the predicted R^2 were maximal, the same predictions were also this model. Furthermore, the other parameter of adequate precision measured the signal-to-noise ratio, this ratio greater than 4 is desirable. Because the obtained adequate precision values were all greater than 4, these results indicated an adequate signal. Therefore, the following quadratic equation was used to navigate the design space according to the predetermined dependent responses.

$$Y = A_0 + A_1X_1 + A_2X_2 + A_3X_1X_2 + A_4X_1^2 + A_5X_2^2$$

Where Y: the dependent response, A_0 - A_5 : the regression coefficients.

The symbol and value of regression coefficients defined the term's tendency and contribution to the response, respectively.^{24,35}

Table 2 Model Summary Statistics of the Selected Responses During Optimization

Parameter	Source	SD	R ²	Adjusted R ²	Predicted R ²	PRESS	F value	Remarks	Adequate Precision
Particle Size	Linear	25.29	0.0002	−0.1998	−1.1951	14.039.53	0.0009		
	2F	24.03	0.1873	−0.0835	−2.0202	19.317.32	2.07		
	Quadratic	11.73	0.8494	0.7418	−0.216	7777.67	15.39		
PDI	Linear	0.07	0.1429	−0.0285	−0.9613	0.1187	0.8337	Suggested	7.1885
	2F	0.07	0.2474	−0.0035	−3.1492	0.2511	1.25		
	Quadratic	0.03	0.8693	0.776	−0.2636	0.0765	16.66		
EE%	Linear	3.58	0.2719	0.1263	−0.6988	299.25	1.87		8.6017
	2F	3.63	0.3268	0.1024	−2.7871	667.14	0.7341		
	Quadratic	2.38	0.7758	0.6156	−0.541	271.47	7.01		
DL%	Linear	0.41	0.9369	0.9242	0.8751	3.38	74.21	Suggested	5.9821
	2F	0.42	0.9404	0.9206	0.8125	5.07	0.5371		
	Quadratic	0.28	0.9794	0.9646	0.876	3.35	6.6		

Response Surface Analysis

Impacts on Particle Size of SLNs

Small-sized particles are essential for orchestration of nanoparticle formulations because this parameter affected the nanoparticles' behavior fates after delivering them into the body.³⁶ The particle size of the prepared SLNs varied from 104.1 nm to 185.5 nm based on the chosen variable levels, indicating a significant influence of these independent variables. The model's quadratic equation for particle size was shown as:

$$Y_1 = 403.57 + 59.18X_1 - 7.57X_2 + 0.27X_1X_2 - 6.26X_1^2 + 0.022X_2^2$$

The Model F-value of 7.90 indicated this model is significant. There was only a 0.85% chance that an F-value this large could occur due to noise. P-values less than 0.0500 indicate that the model terms are significant. In this case, it was found that X_1^2 and X_1X_2 were significant model terms. The analysis showed that the particle size was directly affected by the lipid-to-drug ratio, while it was inversely related to the amount of surfactant. When coefficient values of significant model terms of equation were compared, the interaction term between the lipid-to-drug ratio and surfactant amount showed the greatest influence on size of the generated SLNs. As shown in Figure 1 (I), increasing the lipid-to-drug ratio initially increased particle size but then caused it to decline, forming a saddle shape. No significant change in particle size was observed with variations in the drug-to-lipid ratio, as the particle size of prepared SLNs remained within the nanometer range. As for the influence of surfactant, it was found that the particle size gradually decreased with the increase of surfactant concentration. These results could be attributed to the higher level of surfactants, the lower surface tension. The reduced surface tension between the oil and water phase resulted in nanometer droplets easily formed in the hot aqueous emulsions, consequently the SLNs with the smaller particle size developed after cooling.³⁷

Impacts on PDI of SLNs

The polydispersity index (PDI) is crucial for charactering nanoparticles, reflecting their size distribution heterogeneity or uniformity or not. In the present study, the values of PDI varied from 0.079 to 0.305, indicating a narrow size distribution as most values were below 0.3. The generated equation for PDI is expressed as:

$$Y_2 = 1.57 - 0.053X_1 - 0.022X_2 - 0.000636X_1X_2 + 0.0098X_1^2 + 0.000109X_2^2$$

The model F-value of 9.31 indicated that this model is significant. There was only a 0.53% chance that an F-value this large could occur due to noise. An adequate precision ratio of 8.601 (more than 4) indicated that this model was suitable for navigating the design space. In this case, X_1X_2 , X_1^2 , X_2^2 were significant model terms with this assumption due to their *p*-values less than 0.05, suggesting their importance in the model.

A 3D response surface plot associated with mountain slope shape for description of PDI was presented in Figure 1(II). Increasing the lipid-to-drug ratio initially reduced the PDI, likely due to the inherent emulsification properties of GMS in

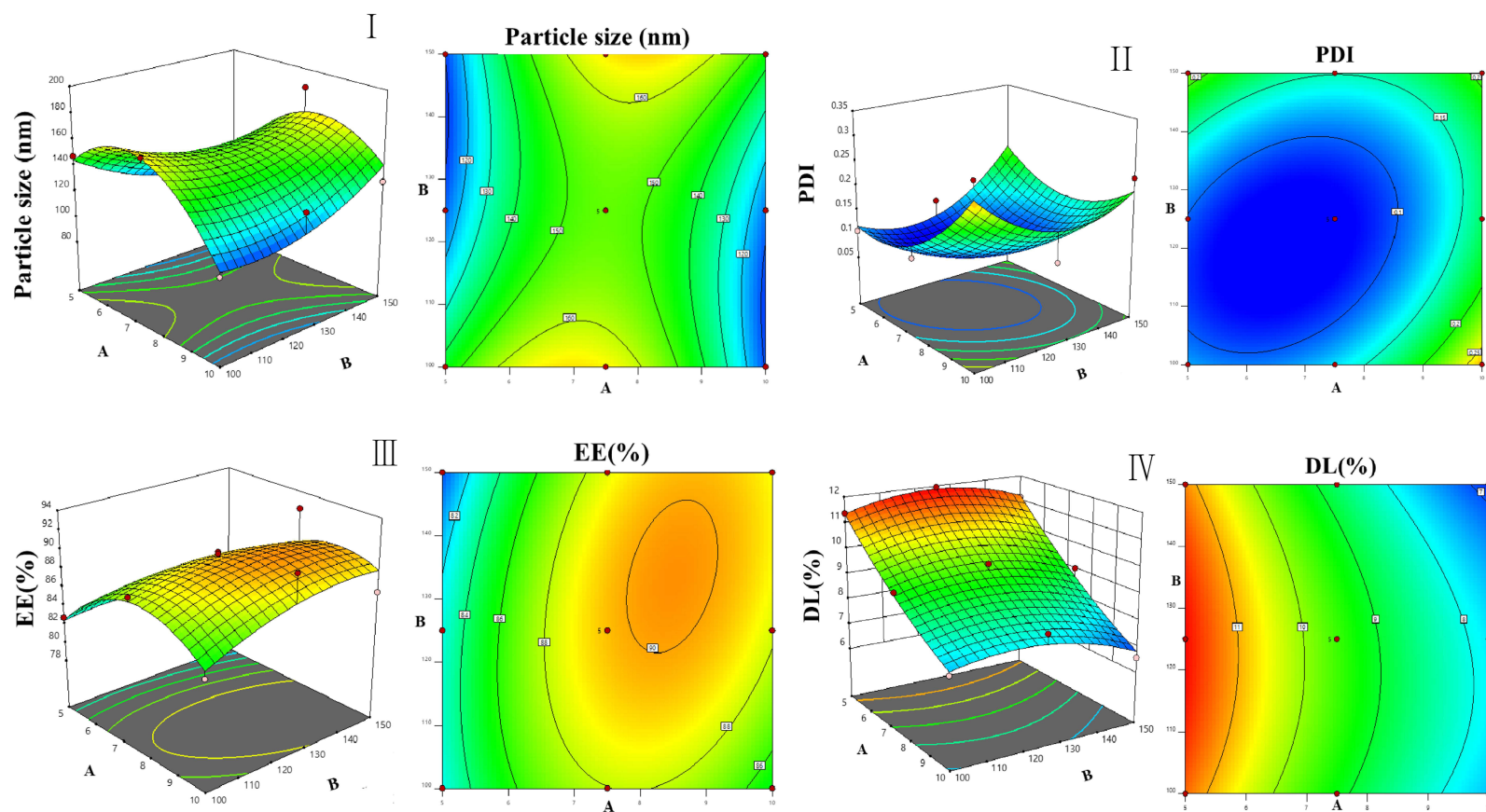


Figure I 3D surface diagrams and contour plots showing the influence of the ratio of lipid to drug (A) and the amount of surfactant (B) on particle size (I); PDI (II); EE(III) and DL(IV) of SLNs.

the lipid. More emulsification potential leads to greater homogeneity;²⁷ However, after reaching a certain point, the PDI began to increase as the lipid-to-drug ratio continued to rise. An abundant lipid matrix led to the agglomeration of solid lipid nanoparticles (SLNs), increasing variability in particle size and resulting in a higher PDI. As for discussing the influence of surfactant amount on PDI, similar results showed that PDI maintained a steady state at first but later it gradually increased with the rise of surfactant. This result could be explained by the fact that the initial surfactant concentration was adequate to reduce the interfacial tension between the dispersed and continuous phases, thus maintaining smaller particle sizes and homogeneity. However, as the amount of surfactants increased further, the developed micelles due to the addition of excessive surfactants resulted in an uneven size distribution in the dispersion system, subsequently causing a higher PDI.

Impacts on EE of SLNs

EE refers to the amount of drugs incorporated into the solid lipid matrix. It is a pivotal indicator of how effectively nanoparticles can deliver enough to the targeted site. In the present study, EE of the 13 runs changed from 78.78% to 92.18%. The quadratic polynomial equation for the measurement EE was as follows.

$$Y_3 = 30.11 + 8.22X_1 + 0.37X_2 + 0.024X_1X_2 - 0.68X_1^2 - 0.022X_2^2$$

The obtained F-value was 4.84 and the *p*-value obtained was 0.0311, indicating only a 3.11% probability that such a large F-value could occur by chance. These values demonstrated that the fitted quadratic model was significant for the specified response. According to ANOVA analysis for quadratic models, the dependent factors X_1 and X_1^2 were significant models due to their *p*-values of less than 0.05.

A sharp convex surface plot for EE was shown in Figure 1(III). It was noted that by increasing the ratio of lipid to drug, a significantly growing inclination of EE appeared; however, as it was continuously increased, a gradual declining trend in EE was observed. A higher lipid ratio provided more excessive space to load additional drug; furthermore, this increased ratio prompted the melted lipid to coagulate quickly, preventing the drug from diffusing into the external aqueous phase and resulting in higher EE.^{38,39} When further increasing the lipid–drug ratio, if it surpassed the range of threshold, which means the lipid cannot accommodate more drugs, continuous increase of the ratio of lipid to drug would decrease the EE.

A slight change of EE showed negligible influence of surfactant on EE as its amount altered. This result was consistent with ANOVA analysis of EE because the influence of model term X_2 was not significant. However, as the surfactant content increased, lower EE was observed due to the formation of micelles, which enhanced drug solubility and led to more drug dissolving in the external aqueous phase, thereby decreasing EE.

Impacts on DL of SLNs

Drug loading is an important parameter that reflects how effectively drugs are incorporated into the SLNs. In the present experiment, the values of DL for the 13 runs changed from 6.56% to 11.94%, suggesting effective ebastine loading in the nanoparticles. A quadratic equation was generated to describe drug loading as follows:

$$Y_4 = 1.95 - 1.24X_1 + 0.25X_2 - 0.0024X_1X_2 + 0.049X_1^2 - 0.000979X_2^2$$

The Model F-value of 66.43 implied that the derived model was significant. There was only a 0.01% chance that an F-value this large could occur due to noise. In this case, P-values of X_1 , X_2^2 less than 0.0500 indicated these model terms were significant. The predicted R^2 of 0.8760 was in reasonable agreement with the adjusted R^2 of 0.9646 as the difference was less than 0.2.

Adequate precision measured the signal-to-noise ratio, where its ratio was 26.479, indicating an adequate signal. Consistently with the regression equation, it was clear that DL was synergistically affected by the ratio of lipid to drug and the interaction term of the content of surfactant.

In Figure 1(IV), it was obvious that the ratio of lipid to drug exerted an opposite effect on DL, a gradual linear declination with increasing levels of ratio of lipid to drug was found. This could be related to the means to calculate the DL, since this value was inversely proportional to the denominator, increasing the lipid-to-drug ratio would raise the

denominator value, thereby reducing the DL. While increasing the surfactant concentration, a minimal decrease effect on DL was observed. Higher levels of surfactants could constrain DL because the used surfactants would promote drug partitioning and render their solubilization in both the lipid and aqueous phases, thus decreasing the DL values.

Optimization and Validation

The recommended formulation was based on predetermined criteria, including minimum goal of particle size and PDI as well as maximum goal of EE and DL. Following these criteria, the optimum formulation of the ebastine-loaded SLNs consisted of a lipid-to-drug ratio of 5.6:1 and 125 mg of surfactant. Therefore, a new batch of ebastine-loaded SLNs was prepared to validate the optimized formulation. The particle size, PDI, EE and DL of the optimized ebastine-loaded SLNs were found to be 147.5 ± 3.32 nm, 0.106 ± 0.005 , $86.7\% \pm 1.55\%$, and $10.02\% \pm 0.18\%$, respectively. These results confirmed the validity of the generated models, as the bias values between the predictive and practical measurements were low ($<15\%$).

Characterization of Ebastine-Loaded SLNs

Particle Size, Zeta Potential and Morphological Observation

Figure 2 showed that the mean particle sizes and zeta potential of the optimized formulation were about 147.5 ± 3.32 nm, -15.1 mV, respectively. These nanoscale particles facilitated oral absorption of ebastine-loaded SLNs, which supported the proposed hypothesis of incorporating ebastine into nanoparticles. The symmetric curve and the less PDI value disclosed narrow size distribution with a normal distribution profile. Zeta potential is a critical parameter for evaluating the stability of SLNs, as it reflects the surface charge and predicts long-term physical stability by indicating the likelihood of aggregation due to electrostatic repulsion. Although the determined value of zeta-

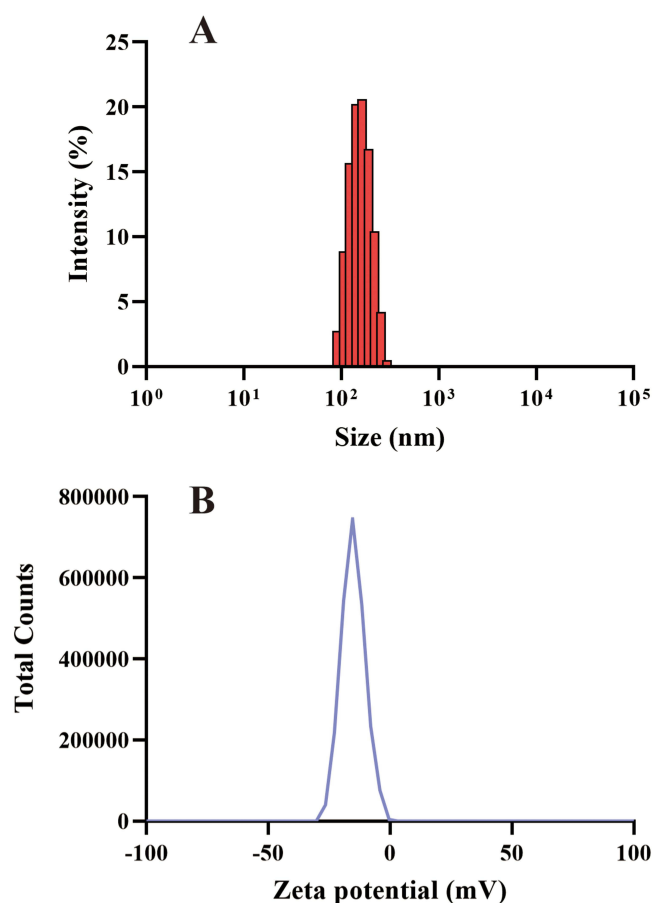


Figure 2 Particle size (A) and zeta-potential (B) of ebastine-loaded SLNs.

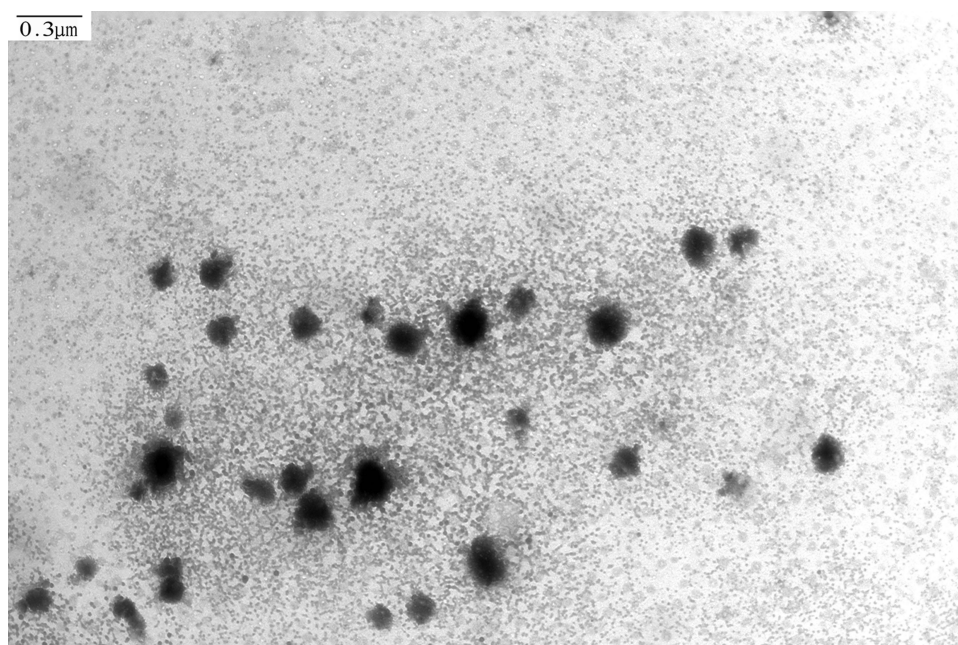


Figure 3 TEM images of ebastine-loaded SLNs.

potential of SLNs is about -15.1 mV, which is lower than that of -30 mV, the stability of SLNs having relative low zeta-potential value results from the steric hindrance mechanism, where the surfactants absorbing on the surface of SLNs hinder the particles' aggregation. The morphology of ebastine-loaded SLNs was observed using TEM, as shown in Figure 3. It showed individual lipid nanoparticles with nearly spherical shapes and without overlapping, having a clear border.

Fourier Transform Infrared Spectroscopy (FTIR)

Figure 4 depicted the typical FTIR spectra of ebastine, the physical mixture (PM), ebastine-loaded SLNs and Blank-SLNs (all similar to EB-SLNs formulation except for the model drug). The distinctive FTIR absorptive peaks of ebastine appeared at wavenumber of 2943 cm^{-1} (attributing to C-H stretching vibration of piperidine ring), 1700 cm^{-1} and 1604 cm^{-1} (representing stretching vibration of C=O (carbonyl group)), 1452 cm^{-1} (due to C=C stretching vibration), 1070 cm^{-1} (contributing to vibration of C-N stretch), respectively. The blank SLNs had remarkable peaks at a wavenumber of 3441 cm^{-1} (the stretching vibration of free OH originated from the lipid matrix structure), 1735 cm^{-1} (attributing to stretching vibration of C=O), 1467 cm^{-1} (contributing to the bending vibration of methyl or methylene group), 1116 cm^{-1} (relating to the stretching vibration of C-O bond). As for the physical mixture of ebastine and blank-SLNs, its FTIR spectrum was developed by merging their spectra together, which both have the special character of ebastine and blank SLNs. While discussing the spectrum of ebastine-loaded SLNs, all typical absorption peaks were found but different from the physical mixture of ebastine and blank-SLNs indicating the absence of any physical or chemical interaction between ebastine and the lipid matrix.⁵

Preparations of ODFs Containing Ebastine-Loaded SLNs

Selection of Film Forming Polymers

An ideal ODFs should possess intact shape without visible roughness or bubbles, have a smooth surface, exhibit better flexibility with good fold endurance to withstand handling without rupture and disintegrate quickly to ensure the rapid release of the loaded drug upon contact with the oral cavity.^{15,40} PVA is generally used as a matrix to prepare films due to its excellent film-forming properties. However, the relatively poor water-soluble feature of PVA restricted its application as a standalone film matrix, since water molecules struggle to penetrate its dense network, leading it slow dissolution.⁴¹ HPMC, as a cellulose ether derivative, has also been explored as film-forming agent with well swelling, flexibility and biocompatibility.^{30,42}

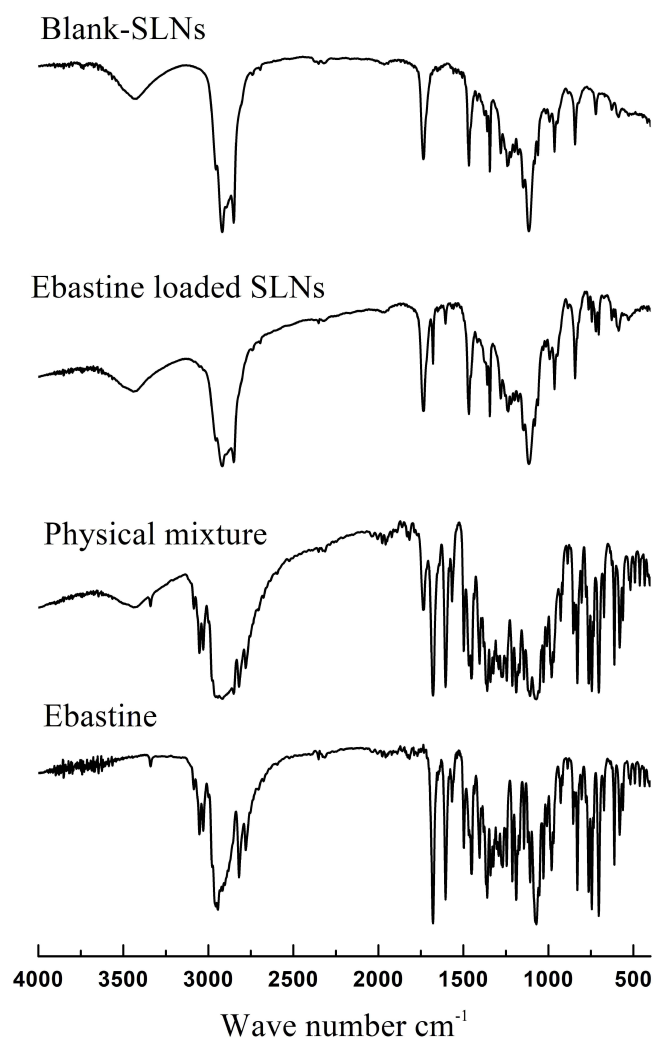


Figure 4 FTIR spectra of blank SLNs, ebastine-loaded SLNs, physical mixture and ebastine.

Introducing another polymer to improve the film's physical property is a helpful strategy to avoid the disadvantage of using only one substrate.⁴³ Habibullah S reported the film's functional properties were ameliorated by mixing PVA and nanocrystalline cellulose together.⁴⁴

In this experiment, different proportions of PVA and HPMC were used to prepare the composite ODFs. Then, the physical appearance, folding endurance and disintegration time of the tailored ODFs were highlighted as the key parameters to describe their properties. The results were shown in [Table 3](#).

As for their physical appearance, the films derived from F3 were soft, semi-transparent with smooth surface compared to the film prepared by other proportions. When the films were fabricated using HPMC alone, it was difficult to peel them off. While using PVA alone, it was hard to spread them smoothly on the glass plate surface and resulted in an uneven surface because this concentration of PVA was too viscous to flow freely.

The folding endurance results disclosed that all films had good mechanical properties as their values of folding endurance were beyond 50 times except for F1 (average 26.67 times). Furthermore, the higher the concentration of PVA in the composite films, the longer the disintegration time. Enhanced folding endurance could be ascribed to the introduction of flexible polymer PVA able to bend easily without breaking. The hydrogen bonds generated from hydroxyl groups among the molecular chains of PVA and HPMC when combinational using them developed a more tight interaction, which extended the disintegration times.⁴⁵

Table 3 Data Normalization for Optimization of ODFs

Batch Code	Physical Appearance	Normali-Zation	Weighted Scores	Folding Endurance	Normali-Zation	Weighted Scores	Disintegration Time	Normali-Zation	Weighted Scores	Total Scores
(PVA: HPMC)	(Scores)	(d_{imax})	(30%)	(Numbers)	(d_{imax})	(35%)	(Seconds)	(d_{imin})	(35%)	(100%)
F1 (0:5)	5.33	0	0	26.67	0	0	87.33	0.87	30.32	30.32
F2 (1:3)	6.67	0.31	9.23	86.33	0.38	13.39	92.67	0.84	29.29	51.90
F3 (1:1)	9.67	1	30	105.33	0.50	17.65	63.33	1	35	82.65
F4 (3:1)	8.33	0.69	20.77	134.33	0.69	24.16	243.00	0	0	44.93
F5 (5:0)	7.67	0.54	16.15	182.67	1	35	181.00	0.35	12.08	63.23

Notes: The final total scores are equal to the sum of each item's normalization value multiply by the corresponding set criteria value.

Data Normalization for Optimization of ODFs

This experiment investigated physical appearance, folding endurance and disintegration time as indicators for formulation optimization. Direct assessment of these results was challenged as the different units used. Here, a criterion normalization method was adopted to transfer them into unified standards without units to eliminate any value dimension effect.⁴⁶

Since all indicators had both positive and negative effects on the target outcome, the normalization formula for variables that should be minimized or maximized,⁴⁷ which calculated as follows:

$$d_{imin} = \frac{Y_{max} - Y_i}{Y_{max} - Y_{min}} \text{ or } d_{imax} = \frac{Y_i - Y_{min}}{Y_{max} - Y_{min}}$$

Where Y_{max} and Y_{min} were the maximum and minimum values of the obtained variables, Y_i was the actual result of each formulation.

According to the predetermined requirements, the evaluation criteria were set as the physical appearance accounting for 30%, folding endurance and disintegration time for 35%, respectively. The final total scores were calculated via summing each item's normalization value multiply by the corresponding set criteria value together, which recorded in Table 3.

In comparison of the total weighted scores among different formulations, the ratio of HPMC and PVA at 1:1 was recommended due to the highest value at this composition.

Characterization of ODFs

pH Measurements

The pH in the oral cavity normally ranged from 6.2 to 7.6, so ODFs that are too acidic or basic could irritate the oral cavity and lead to discomfort, prompting patients to spit them out.⁴⁸ The pH values varied from 6.03 ± 0.02 for F4 to 6.52 ± 0.05 for F1, which was close to that of the oral cavity, suggesting that the prepared ODFs posed minimal irritation. There were no available ionized groups in the polymeric molecular structure altering the pH values. We envisioned that some acidic excipients can be added as pH adjustments because the acidic circumstance could stimulate saliva secretion and subsequently make ODFs disintegrate quickly.

Average Weight and Film Thickness

Measuring the average weight of ODFs ensures film homogeneity since significant weight variation can affect drug content uniformity. The weight of the ODFs ranged from 19.9 ± 0.94 mg to 52.37 ± 0.76 mg. The average weight variation of ODF was attributed to the different amounts of PVA and HPMC used. The largest value for the average weight of the ODF appeared in the case of F5 because the highest concentration of PVA was used in this formulation. The thickness of the ODFs ranged from 32.33 ± 3.68 μ m to 81.33 ± 2.05 μ m, which was in the range of typical ODFs (25–100 μ m). The relatively low SD values disclosed that there was no significant variation in both weight and thickness variation of the prepared ODFs.

Surface Morphology of Films

As presented in Figure 5 A I and B I, the blank ODFs were more transparent than that of ODFs loaded with ebastine SLNs because the photograph of the rooster under the blank ODFs was much clearer than that of the rabbit masked with the other. The introduction of SLNs in the films slightly obstructed light passing through and decreased transparency.

The microstructure of ODFs was shown in Figure 5 A II and B II. The SEM image of ODFs without loading SLNs was overall uniform with an even texture. In comparison, some small round-shaped dots were scattered on the surface of ODFs loading SLNs, indicating SLNs were arranged inside the films. Furthermore, the cross-section images in Figure 5 A III and B III revealed that the ODFs containing SLNs exhibited coarser microstructures compared to the blank ODFs. Most spherical-shaped SLNs were confined within the network of films. No SLNs aggregation was observed in the section of ODFs.

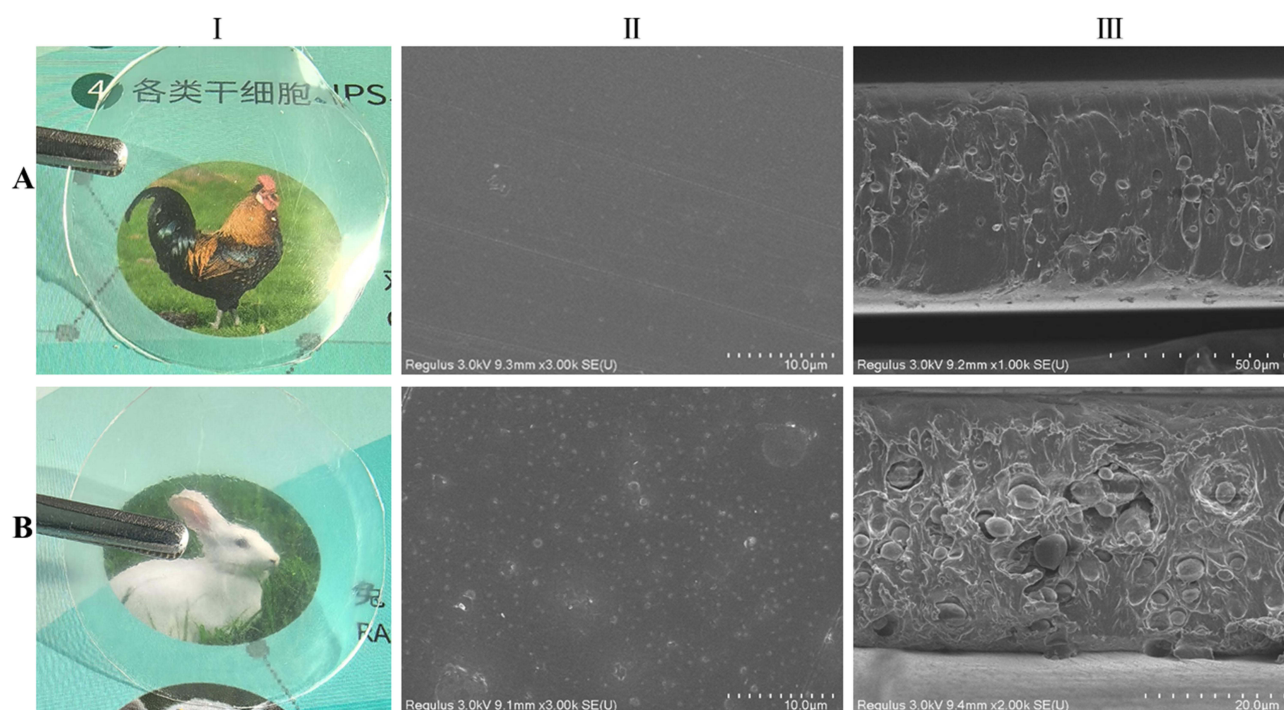


Figure 5 SEM images of ODFs (A) and ODFs with ebastine-loaded SLNs (B).

Reconstitution of ODFs with Ebastine-Loaded SLNs

When placing ODFs into the oral cavity and contacting with saliva, the SLNs were liberated from the film's matrix. The incorporated SLNs in the ODFs should maintain their original nanoparticle properties. Therefore, the released SLNs were evaluated via particle size, and PDI analysis to determine whether the embedded SLN in ODFs can recover to their initially well-dispersed state.

As shown in Figure 6, the particle size increased from approximately 145.06 nm to 190.33 nm after reconstruction. This change indicated that the integrated SLNs were easily recovered to their initial states. The enhanced particle size

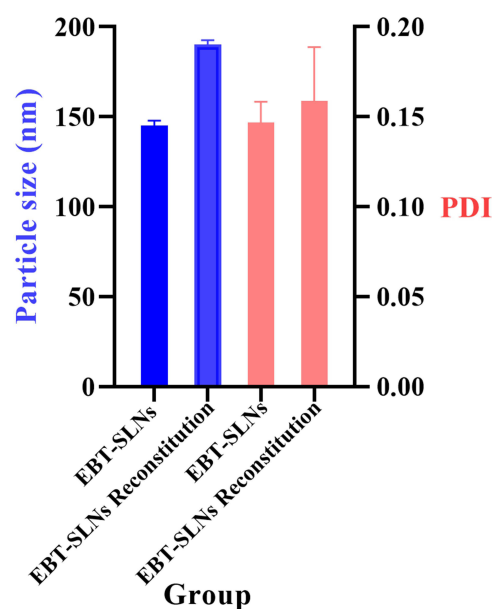


Figure 6 Particle size and PDI of reconstitution of ODFs with ebastine-loaded SLNs.

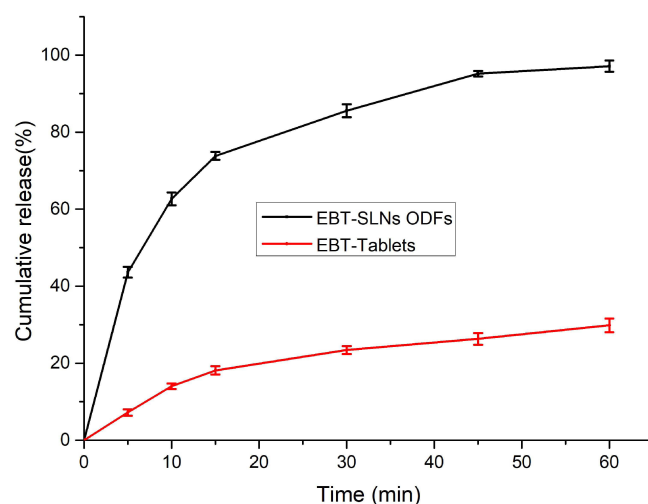


Figure 7 In vitro drug release profile for ODFs with ebastine-loaded SLNs and ebastine tablets.

was ascertained to the adsorption of polymer molecules on the surface of the nanoparticle, correspondingly increasing the hydration radius of them. In addition, the values of PDI were not affected upon integration into the ODFs because there were minimal alterations in the value of PDI, which changed from 0.147 to 0.159 (all less than 0.3). According to paired *t*-test statistical analysis, the *p*-value of particle size change is 0.4507, and the *p*-value of PDI change is 0.2929, indicating that there are no statistical differences in particle size and PDI before and after reconstitution of EBT-SLNs. These results suggested that although ebastine-loaded SLNs were incorporated into the ODFs, they remained their intact nanoparticle properties and homogeneous state after reconstitution without compromising their nanoparticulate properties.

Content Uniformity Determination

The validated HPLC method was constructed to analyze the drug content. The standard curve showed a good linear relationship because the correlation coefficient value of the regression equation was 0.9997. The percentage drug content of three batches of EBT SLNs loaded ODFs ranged from 90% to 110%, confirming that these results meet the required standards. The uniformity was evaluated after determining 10 pieces of films, the value of $A+2.2S$ is 5.04, which complied with the limit (less than 15,) given by Chinese Pharmacopoeia 2020.

In vitro Release Profiles

The in vitro released profiles of ebastine from ODFs loaded with ebastine SLNs and commercial ebastine tablets were depicted in Figure 7. It was found that the drug release patterns from ODFs showed a fast release profile at the early stage and then followed a relatively sustained release over time. When the ODFs contacted the release medium, they quickly disintegrated and subsequently liberated the embedded SLNs. Then the free drug molecules of ebastine deposited on the surface of SLNs accounted for the initially fast release of the drug. After the SLNs are released from the film matrix, the encapsulated drug molecules will gradually be released from the lipid phase, demonstrating a sustained release profile. However, regarding the commercial ebastine tablets, a slower release of drug was found in comparison to that of ODFs. It was observed that less than 30% of ebastine was released after 1 hour, demonstrating an unacceptable released profile. This behavior is due to the poor water-solubility of the model drug, ebastine.

Conclusion

In this study, ebastine-loaded SLNs were successfully formulated and optimized using a central composite rotatable design. After dispersing them into polymer solutions of HPMC and PVA, high-quality oral dissolution films were fabricated, exhibiting excellent physical appearance, mechanical properties, and disintegration time. Furthermore, the SLNs could be well redispersed from the film matrix without compromising their nanoparticulate properties. We

proposed a hybrid platform for the delivery of ebastine by combination of two advanced drug delivery technologies: on the one hand, SLNs was used for improving solubility and bioavailability of the poorly water-soluble model drug, ebastine; on the other hand, ODFs were adopted to enhance patient compliance, enable rapid onset, and circumvent first-pass metabolism. After incorporating ebastine into the lipid matrix, the SLNs' solid lipid core (eg, Compritol 888 ATO and GMS) physically isolated ebastine from hydrolytic/enzymatic degradation in GI fluids, furthermore, surfactants like Poloxamer 188 in SLN formulations reduced interfacial drug exposure, which co-contributed to evading the degradation of ebastine. HPMC and PVA developed dynamic hydrogen bonds between -OH groups, while introducing them in the artificial saliva solution (pH 6.8), bond weakening accelerated polymer erosion and created porous channels, which subsequently released the ebastine-loaded SLNs. Therefore, this research opens new possibilities for integrating solid lipid nanoparticles with oral dissolution films as an effective platform for the delivery of ebastine. This combination not only addresses the solubility and bioavailability challenges associated with ebastine but also provides a user-friendly dosage form that can cater to patients with swallowing difficulties, especially suitability for self-administration and for pediatric or geriatric populations. Consequently, this innovative approach holds significant potential in optimizing the oral administration of ebastine, which offers faster onset and paves the way for improved clinical outcomes for allergy symptom relief. Future work will focus on assessing long-term physical or chemical stability of the ODF-SLN system to consider for industrial application or the feasibility of scale-up. Also, pharmacokinetics as well as pharmacodynamics studies should be performed to demonstrate the potential use of this composite system in the clinic.

Author Contributions

All authors made a significant contribution to the work reported, whether that is in the conception, study design, execution, acquisition of data, analysis and interpretation, or in all these areas; took part in drafting, revising or critically reviewing the article; gave final approval of the version to be published; have agreed on the journal to which the article has been submitted; and agree to be accountable for all aspects of the work.

Disclosure

The authors declare no competing interests.

References

1. Sastre J. Ebastine in the treatment of allergic rhinitis and urticaria: 30 years of clinical studies and real-world experience. *J Investig Allergol Clin Immunol*. 2020;30(3):156–168. doi:10.18176/jiaci.0401
2. Khan BA, Ali A, Hosny KM, et al. Carbopol emulgel loaded with ebastine for urticaria: development, characterization, in vitro and in vivo evaluation. *Drug Deliv*. 2022;29(1):52–61. doi:10.1080/10717544.2021.2015483
3. Islam N, Irfan M, Zahoor AF, et al. Improved bioavailability of ebastine through development of transfersomal oral films. *Pharmaceutics*. 2021;13(8):1315. doi:10.3390/pharmaceutics13081315
4. Roger A, Fortea J, Mora S, Artés M. Ebastine fast-dissolving tablets versus regular tablets: acceptability and preference in patients with allergic rhinitis. *Expert Rev Clin Pharmacol*. 2008;1(3):381–389. doi:10.1586/17512433.1.3.381
5. Kazim T, Tariq A, Usman M, Ayoob MF, Khan A. Chitosan hydrogel for topical delivery of ebastine loaded solid lipid nanoparticles for alleviation of allergic contact dermatitis. *RSC Adv*. 2021;11(59):37413–37425. doi:10.1039/D1RA06283B
6. Islam N, Irfan M, Khan SU, et al. Poloxamer-188 and d- α -tocopheryl polyethylene glycol succinate (TPGS-1000) mixed micelles integrated orodispersible sublingual films to improve oral bioavailability of ebastine; in vitro and in vivo characterization. *Pharmaceutics*. 2021;13(1):54–75. doi:10.3390/pharmaceutics13010054
7. Barve AR, Kapileshwari GR, Dcruz CEM, et al. Solubility enhancement of ebastine by formulating microemulsion using d-optimal mixture design: optimization and characterization. *Assay Drug Dev Technol*. 2022;20(6):258–273. doi:10.1089/adt.2022.049
8. Alvi MN, Khan MA, Waqar MA, Zaman M. Solid lipid nanoparticles: a versatile approach for controlled release and targeted drug delivery. *J Liposome Res*. 2024;34(2):335–348. doi:10.1080/08982104.2023.2268711
9. Katari O, Jain S. Solid lipid nanoparticles and nanostructured lipid carrier-based nanotherapeutics for the treatment of psoriasis. *Expert Opin Drug Deliv*. 2021;18(12):1857–1872. doi:10.1080/17425247.2021.2011857
10. Mirchandani Y, Patravale VB, Brijesh S. Solid lipid nanoparticles for hydrophilic drugs. *J Control Release*. 2021;335:457–464. doi:10.1016/j.jconrel.2021.05.032
11. Steiner D, Emmendorffer JF, B H. Orodispersible films: a delivery platform for solid lipid nanoparticles? *Pharmaceutics*. 2021;13(12):2162. doi:10.3390/pharmaceutics13122162
12. He M, Zhu L, Yang N, Li H, Yang Q. Recent advances of oral film as platform for drug delivery. *Int J Pharm*. 2021;604(1):120759. doi:10.1016/j.ijpharm.2021.120759
13. Hoffmann EM, Breitenbach A, B J. Advances in orodispersible films for drug delivery. *Expert Opin Drug Deliv*. 2011;8(3):299–316. doi:10.1517/17425247.2011.553217

14. Aswathy KV, Beulah KC, Nalina M, et al. Hydroxypropyl methylcellulose stabilized clove oil nanoemulsified orodispersible films: study of physicochemical properties, release profile, mucosal permeation, and anti-bacterial activity. *Int J Biol Macromol.* **2024**;283:137577. doi:10.1016/j.ijbiomac.2024.137577
15. Jacob S, Boddu SHS, Bhandare R, Ahmad SS, N AB. Orodispersible films: current innovations and emerging trends. *pharmaceutics.* **2023**;15(12):2753–2794. doi:10.3390/pharmaceutics15122753
16. Gupta MS, Kumar TP, Gowda DV, Rosenholm JM. Orodispersible films: conception to quality by design. *Adv Drug Deliv Rev.* **2021**;178:113983. doi:10.1016/j.addr.2021.113983
17. Ffoo WC, Khong YM, Gokhale R, Sy C. A novel unit-dose approach for the pharmaceutical compounding of an orodispersible film. *Int J Pharm.* **2018**;539(1–2):165–174. doi:10.1016/j.ijpharm.2018.01.047
18. Xu LL, Shi LL, Cao QR, et al. Formulation and in vitro characterization of novel sildenafil citrate-loaded polyvinyl alcohol-polyethylene glycol graft copolymer-based orally dissolving films. *Int J Pharm.* **2014**;473(1–2):398–406. doi:10.1016/j.ijpharm.2014.07.037
19. Khater ESG, Bahnasawy A, Gabal BA, Abbas W, Morsy O. Effect of adding nano-materials on the properties of hydroxypropyl methylcellulose (HPMC) edible films. *Sci Rep.* **2023**;13(1):5063–5077. doi:10.1038/s41598-023-32218-y
20. Ravasi E, Melocchi A, Arrigoni A, et al. Electrospinning of pullulan-based orodispersible films containing sildenafil. *Int J Pharm.* **2023**;643:123258. doi:10.1016/j.ijpharm.2023.123258
21. Takeuchi Y, Hayakawa F, Takeuchi H. Formulation design of orally disintegrating film using two cellulose derivatives as a blend polymer. *Pharmaceutics.* **2025**;17(1):84. doi:10.3390/pharmaceutics17010084
22. Kozakiewicz-Latała M, Dyba AJ, Marciniak D, et al. PVA-based formulations as a design-technology platform for orally disintegrating film matrices. *Int J Pharm.* **2024**;665:124666. doi:10.1016/j.ijpharm.2024.124666
23. Al-Oran AYF, Yenilmez E. Hydroxypropyl methylcellulose orodispersible film containing desloratadine for geriatric use: formulation and evaluation. *Antiinflamm Antiallergy Agents Med Chem.* **2023**;22(2):79–91. doi:10.3390/nano9020230
24. Narendar D, Karthik Y. Lipid nanoparticles of zaleplon for improved oral delivery by Box–Behnken design: optimization, in vitro and in vivo evaluation. *Drug Dev Ind Pharm.* **2017**;43(7):1205–1214. doi:10.1080/03639045.2017.1304957
25. Chirio D, Peira E, Dianzani C, et al. Development of solid lipid nanoparticles by cold dilution of microemulsions: curcumin loading, preliminary in vitro studies, and biodistribution. *Nanomaterials.* **2019**;9(2):230–247.
26. Mishra R, Jain N, Kaul S, N U. Central composite design-based optimization, fabrication, and pharmacodynamic assessment of sulfasalazine-loaded lipoidal nanoparticle-based hydrogel for the management of rheumatoid arthritis. *Drug Deliv Transl Res.* **2023**;13(4):994–1011. doi:10.1007/s13346-022-01260-0
27. Talarico L, Pepi S, Susino S, et al. Design and optimization of solid lipid nanoparticles loaded with triamcinolone acetone. *Molecules.* **2023**;28(15):5747. doi:10.3390/molecules28155747
28. Łe CK, Sznitowska M, Sznitowska M. Technology of orodispersible polymer films with micronized loratadine-influence of different drug loadings on film properties. *Pharmaceutics.* **2020**;12(3):250–265. doi:10.3390/pharmaceutics12030250
29. Vlad RA, Pinte A, Coaicea M, et al. Preparation and evaluation of caffeine orodispersible films: the influence of hydrotropic substances and film-forming agent concentration on film properties. *Polymers.* **2023**;15(9):2034–2053. doi:10.3390/polym15092034
30. Pacheco MS, Barbieri D, da Silva CF, De Moraes MA, MA dM. A review on orally disintegrating films (ODFs) made from natural polymers such as pullulan, maltodextrin, starch, and others. *Int J Biol Macromol.* **2021**;178:504–513. doi:10.1016/j.ijbiomac.2021.02.180
31. Agubata CO, Mbah MA, Akpa PA, U G. Application of self-healing, swellable and biodegradable polymers for wound treatment. *J Wound Care.* **2021**;30(Sup9a):IVi–IVx. doi:10.12968/jowc.2021.30.Sup9a.IV
32. Takeuchi Y, Ikeda N, Tahara K, Takeuchi H. Mechanical characteristics of orally disintegrating films: comparison of folding endurance and tensile properties. *Int J Pharm.* **2020**;589:119876. doi:10.1016/j.ijpharm.2020.119876
33. Scarpa M, Paudel A, Klopogge F, et al. Key acceptability attributes of orodispersible films. *Eur J Pharm Biopharm.* **2018**;125:131–140. doi:10.1016/j.ejpb.2018.01.003
34. Mm SM, Mehanna MM. Disintegration time of orally dissolving films: various methodologies and in-vitro/in-vivo correlation. *Pharmazie.* **2019**;74(4):227–230. doi:10.1691/ph.2019.8231
35. Emami J, Mohiti H, Hamishehkar H, V J. Formulation and optimization of solid lipid nanoparticle formulation for pulmonary delivery of budesonide using Taguchi and Box–Behnken design. *Res Pharm Sci.* **2015**;10(1):17–33.
36. Raja HN, Din FU, Shabbir K, et al. Sodium alginate-based smart gastro-retentive drug delivery system of revaprazan loaded SLNs; Formulation and characterization. *Int J Biol Macromol.* **2023**;253(Pt.6):127402. doi:10.1016/j.ijbiomac.2023.127402
37. Ali HSM, Namazi N, Elbadawy HM, et al. Repaglinide–solid lipid nanoparticles in chitosan patches for transdermal application: box–behnken design, characterization, and in vivo evaluation. *Int J Nanomed.* **2024**;19:209–230. doi:10.2147/IJN.S438564
38. Hao J, Fang X, Zhou Y, et al. Development and optimization of solid lipid nanoparticle formulation for ophthalmic delivery of chloramphenicol using a Box–Behnken design. *Int J Nanomed.* **2011**;6:683–692. doi:10.2147/IJN.S17386
39. Sanad RA, Abdelmalak NS, Elbayomy TS, B AA. Formulation of a Novel Oxybenzone-Loaded Nanostructured Lipid Carriers (NLCs). *AAPS Pharm Sci Tech.* **2010**;11(4):1684–1694. doi:10.1208/s12249-010-9553-2
40. Speer I, Steiner D, Thabet Y, Breitzkreutz J, K A. Comparative study on disintegration methods for oral film preparations. *Eur J Pharm Biopharm.* **2018**;132:50–61. doi:10.1016/j.ejpb.2018.09.005
41. Huang J, Chen M, Zhou Y, Li Y, H Y. Functional characteristics improvement by structural modification of hydroxypropyl methylcellulose modified polyvinyl alcohol films incorporating roselle anthocyanins for shrimp freshness monitoring. *Int J Biol.* **2016**;8:10–21. doi:10.5539/ijb.v8n3p10
42. Ya GVS, Dias RJ. Citric acid crosslinked cyclodextrin/hydroxypropylmethylcellulose hydrogel films for hydrophobic drug delivery. *Int J Biol Macromol.* **2016**;93(Pt A):75–86. doi:10.1016/j.ijbiomac.2016.08.072
43. Jadach B, Misek M, Ferlak J. Comparison of hydroxypropyl methylcellulose and alginate gel films with meloxicam as fast orodispersible drug delivery. *Gels.* **2023**;9(9):687. doi:10.3390/gels9090687
44. Habibullah S, Swain R, Nandi S, et al. Nanocrystalline cellulose as a reinforcing agent for poly (vinyl alcohol)/ gellan-gum-based composite film for moxifloxacin ocular delivery. *Int J Biol Macromol.* **2024**;270(Pt 1):132302. doi:10.1016/j.ijbiomac.2024.132302
45. Voronova MI, Surov OV, Guseinov SS, Barannikov VP, Z AG. Thermal stability of polyvinyl alcohol/nanocrystalline cellulose composites. *Carbohydr Polym.* **2015**;130:440–447. doi:10.1016/j.carbpol.2015.05.032

46. Zhang W, Parniak MA, Sarafianos SG, Cost MR, Rohan LC. Development of a vaginal delivery film containing EFdA, a novel anti-HIV nucleoside reverse transcriptase inhibitor. *Int J Pharm.* 2014;461(1–2):203–213. doi:10.1016/j.ijpharm.2013.11.056
47. Hassan EE, Parish RC, G JM. Optimized formulation of magnetic chitosan microspheres containing the anticancer agent, oxantrazole. *Pharm Res.* 1992;9(3):390–397. doi:10.1023/A:1015803321609
48. Bharti K, Mittal P, Mishra B. Formulation and characterization of fast dissolving oral films containing buspirone hydrochloride nanoparticles using design of experiment. *J Drug Deliv Sci Technol.* 2019;49:420–432. doi:10.1016/j.jddst.2018.12.013

International Journal of Nanomedicine

Publish your work in this journal

The International Journal of Nanomedicine is an international, peer-reviewed journal focusing on the application of nanotechnology in diagnostics, therapeutics, and drug delivery systems throughout the biomedical field. This journal is indexed on PubMed Central, MedLine, CAS, SciSearch®, Current Contents®/Clinical Medicine, Journal Citation Reports/Science Edition, EMBase, Scopus and the Elsevier Bibliographic databases. The manuscript management system is completely online and includes a very quick and fair peer-review system, which is all easy to use. Visit <http://www.dovepress.com/testimonials.php> to read real quotes from published authors.

Submit your manuscript here: <https://www.dovepress.com/international-journal-of-nanomedicine-journal>

Dovepress
Taylor & Francis Group